Design of Sub-THz Slotted Waveguide Array Antenna for the Broadside Circularly Polarized Applications Beyond 5G

Thevaruparambil A. Nisamol[*], Parambil Abdulla, and Kunnath K. Ansha

Abstract—This work presents the modelling of a highly efficient all-metal slotted waveguide array antenna (SLWA) at sub-THz frequencies for the 5th generation communication applications or beyond. The slotted waveguide array antenna is modified for the accomplishment of high gain, wide bandwidth, and circularly polarized broadside radiation pattern. The proposed double 'T'-shaped slot (DTS) which acts as an active element in the whole antenna radiation and other elements after DTS contribute high directivity and gain. The designed slotted waveguide array antenna with DTS is modified for the reconfiguration of linear polarization into circular polarization and achieves the axial ratio (AR) below 3 dB for the bandwidth of 22.323 GHz with a maximum gain of 14.4 dBi. The length and shape of the slots are altered in the SLWA in-order to set up the advanced rectangular stepdown slots (RSDS) and cross stepdown slots (CSDS) for the circularly polarized beam scanning application. The RSDS SLWA, and CSDS SLWA provide wide impedance bandwidths of 56.506 GHz and 61.236 GHz with 3 dB AR range of 12.417 GHz and 9.688 GHz, respectively. The design and simulation of the proposed antenna are done in CST microwave suite and validated using HFSS software.

1. INTRODUCTION

In recent years, the sub-THz range of frequencies offers ultra-fast and high signalling wireless communications for future 5G/6G applications. The huge demand in the frequency spectrum for long-distance communication and extended data rate requirements causes capacity constraints and insufficient spectrum resources. In this scenario, the sub-THz frequency band which is unconsumed by commercial and industrial applications will be able to meet the future tremendous wireless communication requirements beyond 5G. There are numerous works in progress for the utilization of fast-developing sub-terahertz spectrum which demands properly working antennas and systems at this range. The huge demand in the sub-THz spectrum leads to the development of different types of approaches in the waveguide antennas. The antenna arrays with different architectures such as metal waveguides [1], dielectric rod waveguides [2], and substrate integrated waveguides (SIW) are investigated for the emerging indoor multiuser applications for the reduction of insertion loss occurred at the sub-THz frequencies. To accomplish the highly developing requirements in this frequency range, a low temperature cofired ceramic substrate (LTCC) is used as a package [3] which can increase the bandwidth using SIW technology [4, 5]. For the short-range communication systems at sub-THz frequencies, the LTCC technology can be used as a package to suppress the electromagnetic leakage. However, at lower pressures (50 and 100 atmospheres), ceramics tape layers show a lack of integration in between.

There are lots of emerging wideband wireless applications such as PCS, UMTS, WiFi, WiMAX which require stable broadside radiation pattern with higher gain. The radiated arrays are designed using slots or the deposition of metal strips on the planar dielectrics for the highly directive stable broadside radiation. Yagi-Uda antennas [6, 7] are the most common antennas that can be

* Corresponding author: Thevaruparambil A. Nisamol (nisamolshiyas2018@cusat.ac.in).
The authors are with the School of Engineering, Cochin University of Science and Technology, India.

effectively utilized to achieve these characteristics. For low-frequency ISM (Industrial, Science, Medical) applications, Yagi-Uda broadside antenna radiation is extensively employed using coplanar stripline. Even so, it is hard to realize high gain and wideband stable broadside radiation pattern simultaneously. For radar beam scanning applications, printed broadside antenna arrays [8] have obtained wide attention for the accomplishment of superior characteristics. For broadside array elements, current distribution possesses a major role in the radiation pattern, and the unequal element currents indicate significant pattern variations [9]. The beam scanning presented in [10] was accomplished using leaky-wave SIW technique for the consistent and high gain radiation pattern.

In the printed antenna design, planar leaky-wave elements offer low cost and directive broadside radiation for the wireless power transmission applications at 5G communication frequencies [11, 12]. However, from the past years, broadside radiation was analysed for the stopband behaviour occurred at the beam scanning direction. It leads to an increase in the attenuation of leakywave as the broadside beam tends to cover scan angle on either side especially at higher band frequencies.

Besides the planar printed structures, it is very much effective in utilizing all-metal waveguide structures for the realization of stable high gain broadside radiation pattern under sub-THz frequencies. The highly efficient and consistent radiation can be realized using radiated slots in waveguide paradigms. The discontinuities in the metal sheet bring the radiation to the free space with a significant increase in directivity and gain due to the absence of losses encountered by the dielectric materials. The polarization of the antenna attains immense importance in the high data rate applications. Moreover, the linearly and circularly polarized antennas possess various utilization in every frequency band. The wide acceptance of circularly polarized (CP) waves by several applications such as satellite communication, military radar range detection are due to the reduction in the polarization mismatch and multipath interference. The dielectric substrate with optimized patch dimensions is commonly available for acquiring CP waves at wide range of frequencies [13–16]. The higher operating frequency for the CP antenna with wide axial ratio bandwidth is highly in demand. Most of the literatures published in CP antennas are at lower band of frequencies. The CP radiation is achieved by various slot shapes such as tapered slot [17], square-shaped slot [18], S-shaped slot [19], triangular slot [20], electrically scanned slot [21], centre cross slots [22, 23], and rectangular slots [24]. These structures provide confined impedance bandwidth with poor efficiency. Furthermore, substrate integrated waveguide technologies and microstrip structures are also furnished at frequency band above 50 GHz to maintain low axial ratio with CP radiation pattern [25, 26]. They have reduced band of circular polarization over the entire impedance bandwidth and show poor radiation efficiency with lower gain. The circularly polarized radiation towards different scan angles also finds many applications in the communication areas. Beam steering antennas are designed using several methods such as planar radiating elements [27], phased array [28], Luneburg lens array [29], waveguide slotted array [30], and slotted SIW [31]. The CP-beam steering antennas established using the metallic waveguide slots which operate in the sub-THz frequencies are highly effective as the losses are minimum.

In the slotted array antenna, each slot having different lengths is radiated for different frequencies at different angles, since the length of the slots depends on the resonant frequencies. The beam scanning array of slots on the metal waveguides provides higher power handling capacity and can be designed for rigid environmental conditions [28]. The beam scanning approach in the metal waveguides can be accomplished using different slot lengths. Each slot provides the major beam towards different angles, and they have a crucial requirement in the radar communication. Since there is a high loss factor in the sub terahertz frequencies, it is hard to observe circular polarization and lower axial ratio for a huge band of frequencies.

In this article, a circularly polarized slotted waveguide array antenna with narrow beam scanning at sub-THz frequencies is accomplished. A stable broadside radiation pattern is achieved with different kinds of slots on the WR3 waveguide enclosed within a metal cabin. The high gain radiated slots after double 'T'-shaped slot (DTS) are designed to obtain higher bandwidth of 61.5 GHz and 96.74% efficiency. The cross slots after DTS achieve circular polarization of 36.44% of the impedance bandwidth which ranges from 257 GHz to 321 GHz with a maximum gain of 14.4 dBi. The slotted dimensions are adjusted to obtain two paradigms of beamforming slotted array with impedance bandwidth of 56.5 GHz and 61.2 GHz having wideband circular polarization for 21.974% and 15.820% of the impedance bandwidth, respectively. In the article, Section 1 depicts the design of linearly polarized slotted array waveguide

antenna with a metal cabin. Section 2 gives the design of circularly polarized waveguide antenna with an array of cross slots. The beamforming slotted designs for CP are detailed in Section 3. The major results of the waveguide antenna are obtained in CST microwave studio and verified using HFSS software.

2. SLOTTED WR3 WAVEGUIDE

The WR3 waveguide having recommended frequency band between 220 GHz and 340 GHz with dimensions 0.8636 mm × 0.4318 mm is employed for the design of a sub-THz SLWA. To achieve minimum signal loss and attenuation at this frequency range, the microwave signal processing components should be of high accuracy within compact dimensions. Since WR3 is a waveguide having ultra-small dimensions, the fabrication using CNC metal milling machines [32] finds it more difficult, and it is hard to design complicated structures inside these waveguides. To solve this problem and for the easiness of fabrication, the slotted array of antenna is proposed and designed on WR3 waveguide. The increasing demand for THz antenna applications can be met by using this technique. The frequencies around 300 GHz are highly developing in the communication field due to the over utilization of lower frequencies by the industrial and communication applications. In the design of SLWA, single linearly polarized transverse slot for 280 GHz is optimized initially, and Figure 1 shows the physical dimensions of the WR3 waveguide. Table 1 gives the designed dimensions of the single slotted waveguide.
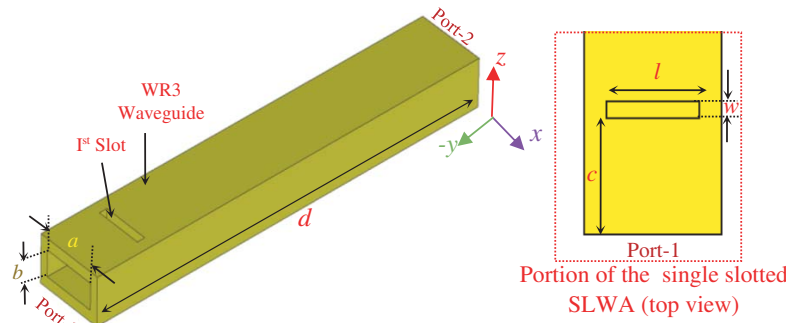

Figure 1. WR3 slotted waveguide dimensions (perspective view and portion of top view).

Table 1. The designed dimensions of a single slotted section.

Dimensions	Values (mm)
a	0.8636
b	0.4318
c	0.9195
d	5.6
w	0.1
l	0.58

3. LINEARLY POLARIZED SLOTS

The slots are created on the transverse direction of the waveguide for implementing maximum radiation at 280 GHz frequency. The proposed work focuses on broadside radiation pattern using the slotted array. The linearly polarized slots are arranged in a coplanar way, and the second slot is modified into a double 'T' shaped slot (DTS) which acts as an active element and improves the radiation characteristics of the entire slotted array. Figure 2(a) illustrates the design of DTS on SLWA, and Figure 2(b) shows

a slotted waveguide array antenna with DTS separated by a distance 'h' greater than $\lambda/10$, where 'λ' is the free space wavelength. The lengths of the slots 'l' are designed for $\lambda/2$ and optimized for slightly higher values of half wavelength. In Figure 2(c), the minimum reflection loss at the resonant frequency is observed without DTS compared with the proposed SLWA with DTS. Hence the designed DTS is found imperative for the whole antenna radiations, and the device is highly matched. The optimized dimensions of DTS are given in Table 2. The SLWA is placed inside a metal cabin which is constructed by bending the sides of a metal sheet having thickness of 0.1 mm as shown in Figure 3(a). The gain and bandwidth are augmented in this structure, and the results are compared in Figure 3(b). Impedance bandwidth of the SLWA with metal cabin is observed as 61.5 GHz (from 262.5 GHz to 324 GHz) which shows an enhancement of 13 GHz from the reflection characteristics of SLWA without metal cabin.
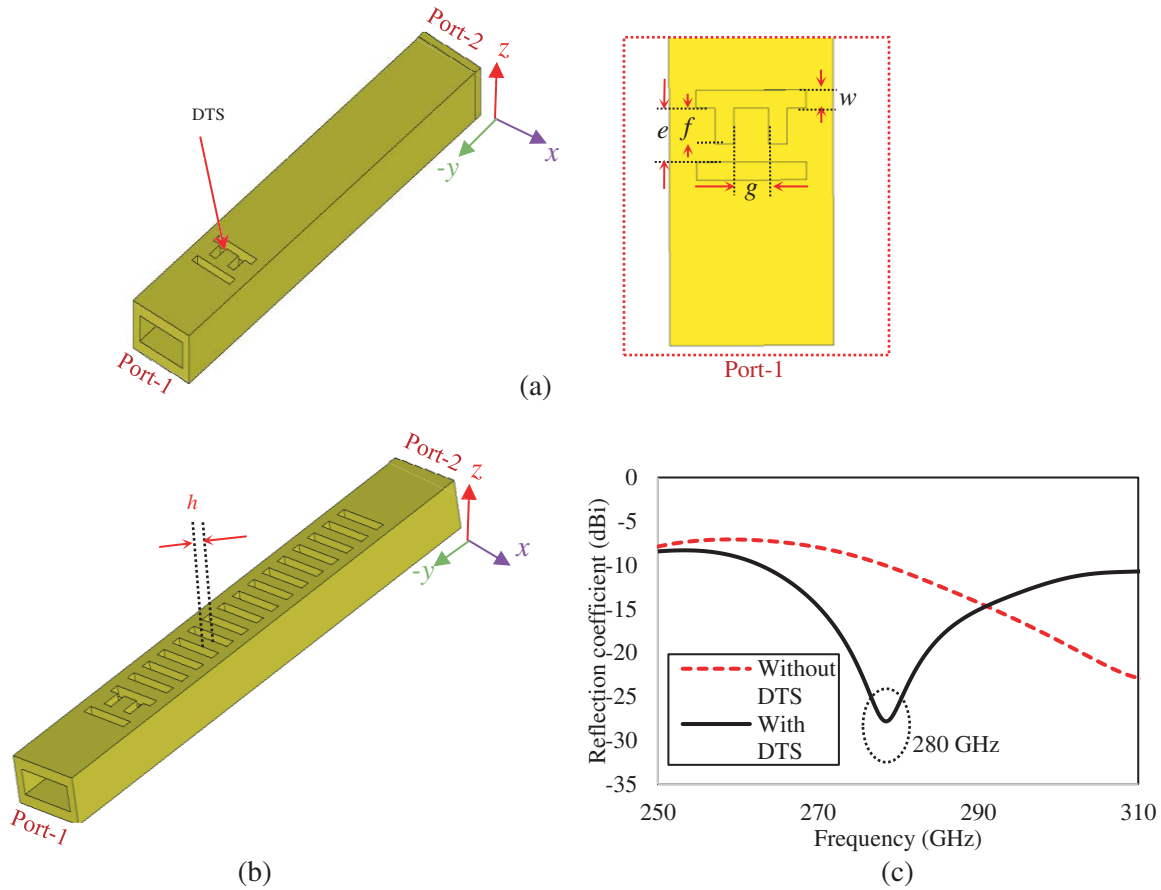

Figure 2. (a) Design of double 'T' shaped slot (Perspective view and a section of top view). (b) Perspective view of linearly polarized slots with DTS (c) Comparison between the slotted waveguide array with and without active DTS.

Table 2. The designed dimensions of slotted broadside array with DTS.

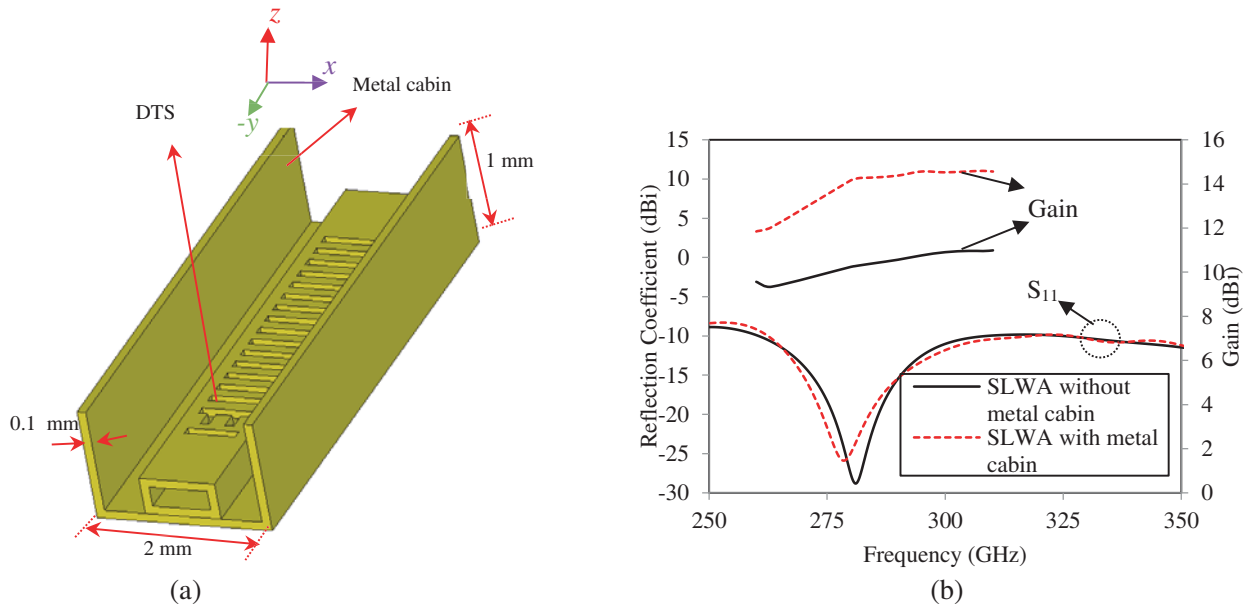| Dimensions	Values (mm)
e	0.3
f	0.2
g	0.205
h	0.125

Figure 3. (a) SLWA with metal cabin. (b) Simulation result comparison between SLWA with and without metal cabin.
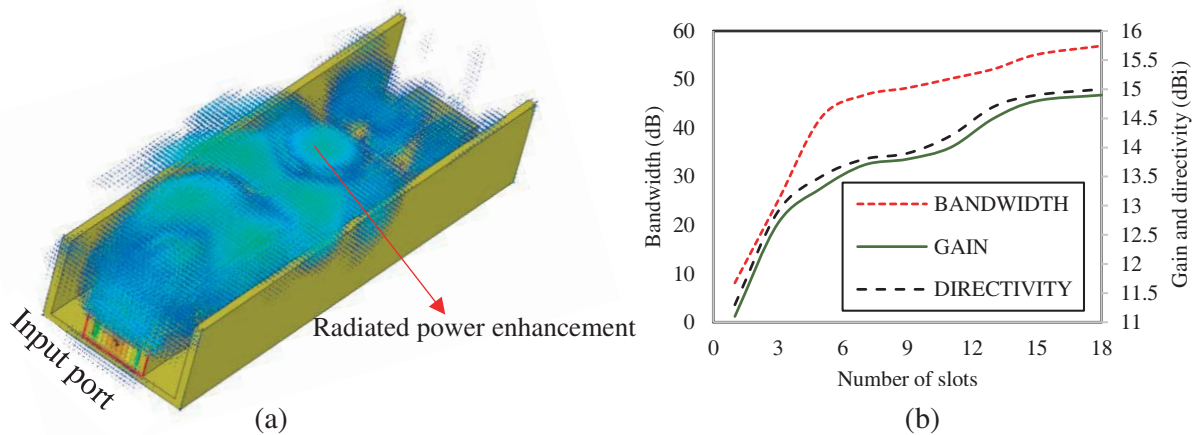

Figure 4. (a) The field distribution on the SLWA with metal cabin. (b) Effects of slots on gain, bandwidth and directivity of SLWA with metal cabin.

For the proposed waveguide array with metal cabin, an increase in the maximum gain of 4 dBi is observed compared to SLWA without metal cabin. The metal cabin enhances radiation towards the main lobe and improves the directivity to 14.4 dBi at 280 GHz. Since the dimensions of the waveguide at sub-THz frequencies are very compact, the metal cabin provides a metal platform for the easy handling of the structure and can be used for platform embedded applications. It also serves as a back cavity with reflected power combining [33] with the radiated power at the output radiation as seen from the 3D field distribution diagram in Figure 4(a). The number of slots after the DTS influences the performance characteristics of SLWA. The reflection coefficient characteristics are analysed for different numbers of slots, and the variations of gain and directivity along with the bandwidth are plotted in Figure 4(b). It is observed that there is no significant advancement in the maximum gain for the further increase in the number of slots beyond 15.

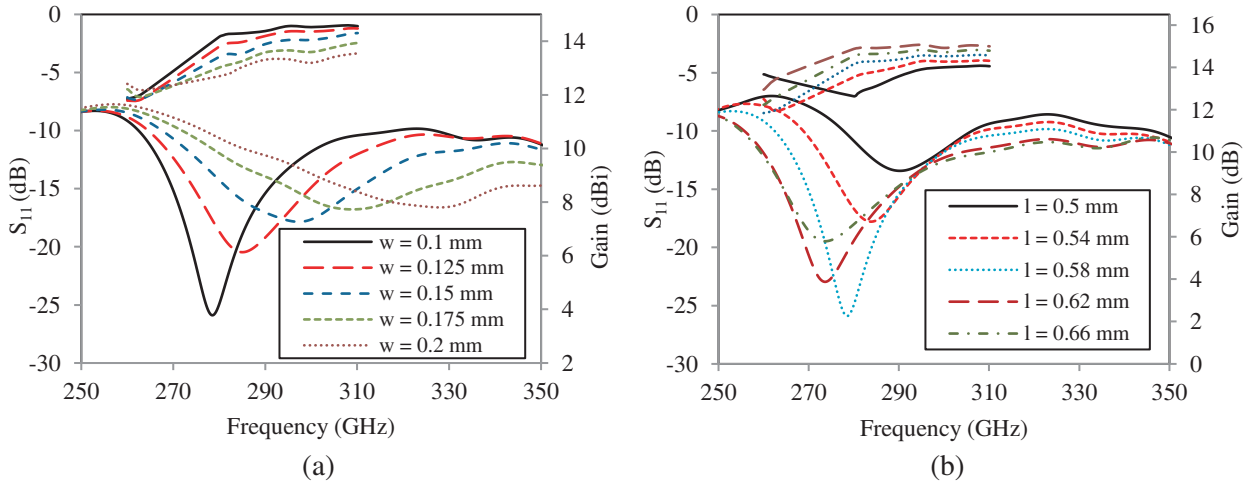The slots added after DTS act as directors as well as radiating element in the SLWA. They partially

Figure 5. Parametric optimization of linear slots. (a) Width of the slots ('*w*'). (b) Length of the slots ('*l*').
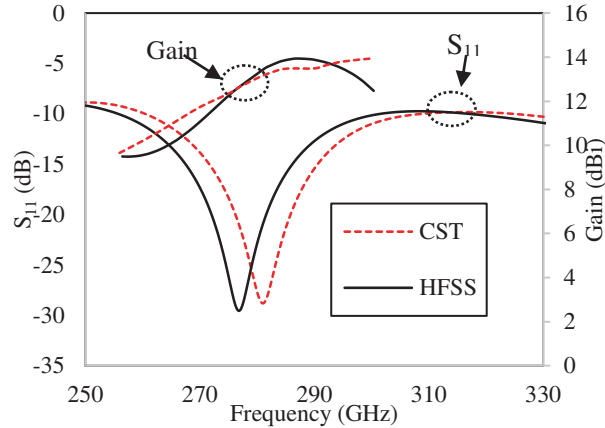

Figure 6. Simulation verification using CST and HFSS software for the linearly polarized SLWA.

contribute to the enhancement of radiation pattern after 6 slots.

The slot dimensions of the SLWA are parametrically optimized as shown in Figures 5(a), (b). Since the slots in the SLWA function as active radiating elements, the length and width of the slot possess remarkable impact on the characteristics of the antenna. After considering the gain and S11 characteristics, the width of the slot is optimized to 0.1 mm for the proposed resonant frequency. It is indicated that the maximum coupling between the slotted array elements are obtained at 0.1 mm width. The increase in the width of the slot comes up with notable reduction in the gain, and shift occurs from the frequency of interest. The length of the slot is designed as '*l*' slightly greater than $\lambda/2$ and optimized to 0.58 which is a compromise between the impedance bandwidth and magnitude of the reflection coefficient. Figure 6 compares the simulation results of SLWA with metal cabin using two commercially available softwares, CST and HFSS.

The E plane and H plane radiation patterns of linearly polarized SLWA with $\varphi = 90°$ and $\varphi = 0°$ are shown in Figures 7(a) and (b). The stable broadside patterns for different frequencies are observed in Figure 8. The main lobe level of 14.8 dBi is observed with a minimum sidelobe level of 1.9906 dBi. The simulated co- and cross-polar radiation patterns at the centre frequency of 280 GHz exhibit excellent isolations of 105.4 dB and 111.9 dB in the boresight direction for the E-plane and H-plane, respectively. It also shows a 30° angular shift in the realized broadside gain pattern [15] for the range of frequencies within the bandwidth. The co- and cross-polar radiation patterns are also analysed using HFSS software
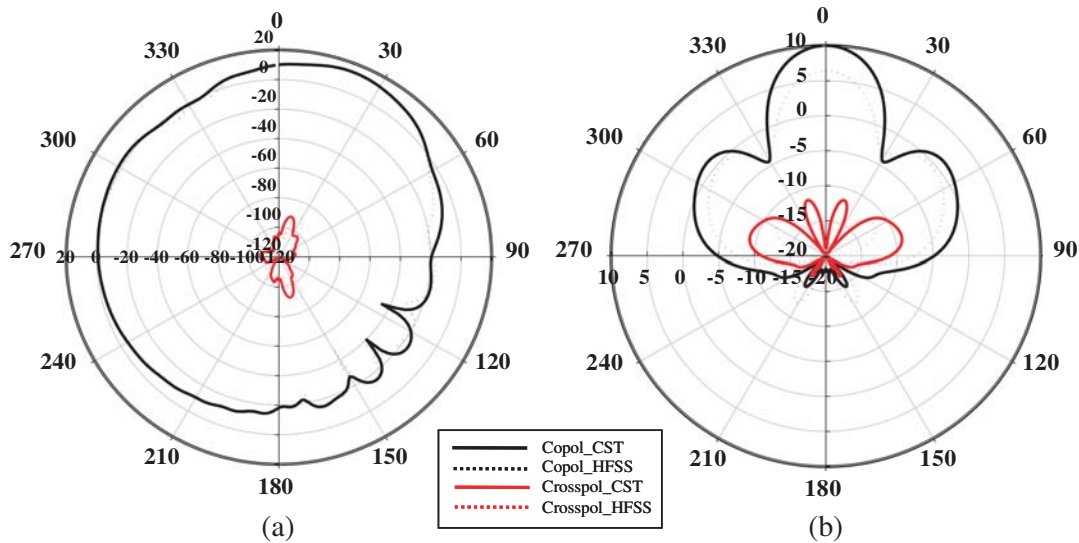
Figure 7. Electric field radiation pattern at 280 GHz (a) E plane ($\varphi = 90°$). (b) H plane ($\varphi = 0°$).

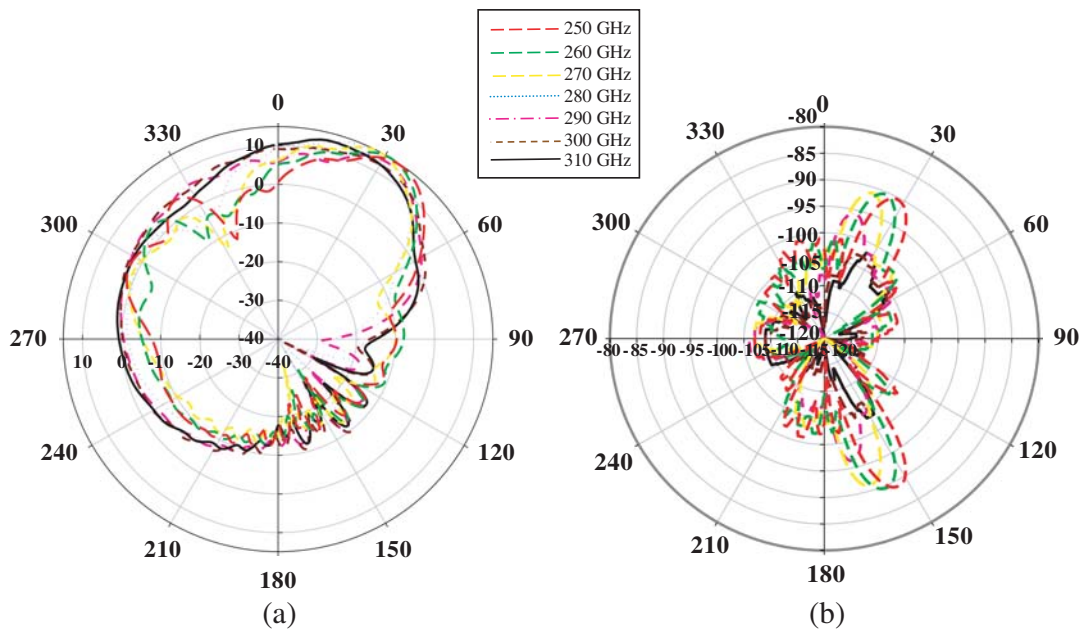**Figure 8.** Stable broadside E-plane radiation pattern at $\varphi = 90°$ for different frequencies. (a) Copolar pattern. (b) Cross polar pattern.

which verifies the practical accuracy of the simulated results. The 3-dB beamwidth of 18.132° towards shifted z-axis is achieved along with the antenna radiation efficiency of 96.74%.

4. CIRCULARLY POLARIZED SLOTS

There are diverse applications for circular polarization since the orientation of the antenna at the receiver side is hardly affected. The circularly polarized radiation is provided by the angular shifted cross slots (CRS) placed after DTS which is transverse to the waveguide. The design of angular shifted CRS is accomplished by rotating the linear slots towards $K = +20°$ and $K = -20°$ one after the other and forming eight CRS sections followed by DTS as shown in Figure 9(a). The reflection coefficient

(a)   (b)
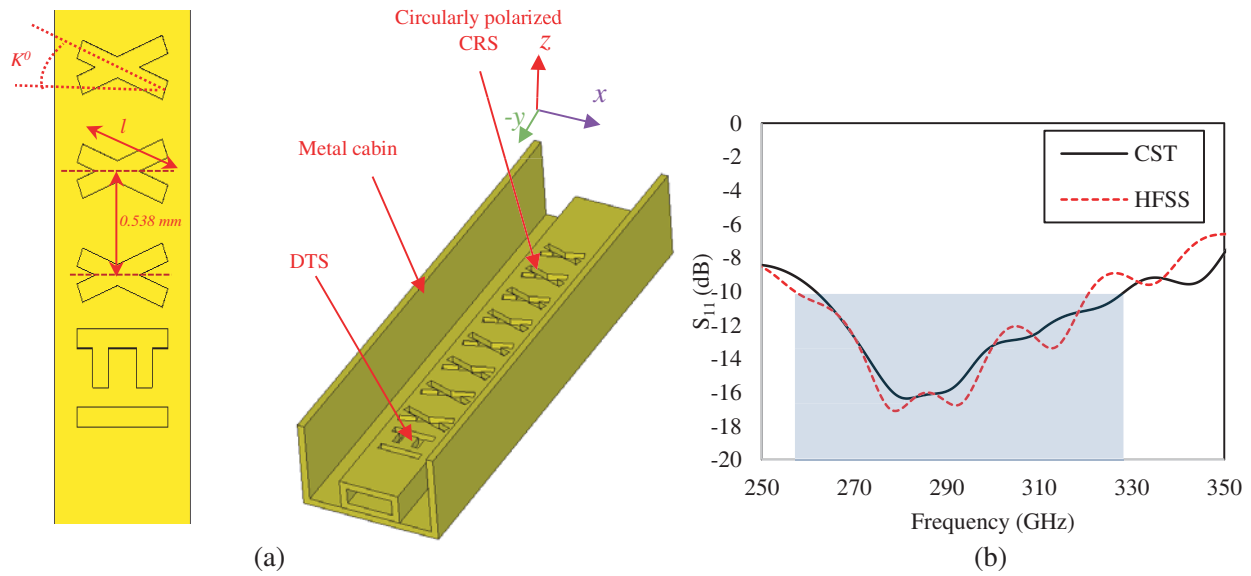
Figure 9. (a) Circularly polarized slot design (top and perspective view) for SLWA. (b) Reflection coefficient characteristics over the bandwidth in CST and HFSS software.
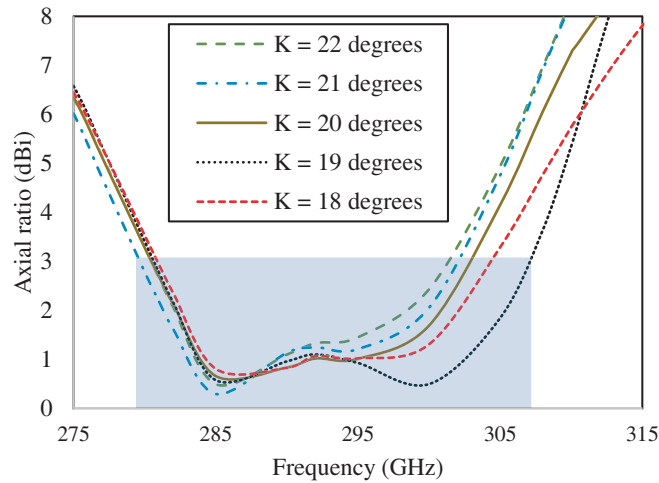

Figure 10. The parametric analysis of 3 dB axial ratio bandwidth.

characteristics are plotted in Figure 9(b), and it is observed that maximum impedance bandwidth of 64 GHz beyond -10 dB attenuation is accomplished from 257 GHz to 321 GHz. The axial ratio is parametrically analysed in Figure 10, and it is observed that marginal variation of the rotating angle gives rise to the reduction of axial ratio bandwidth. The optimized angle of $20°$ is preferred due to the effect of minimum gain for other angles. The circular polarization is accomplished for 23.323 GHz bandwidth (from 280.89 GHz up to 304.21 GHz) which is 36.44% of the actual bandwidth from the 3-dB axial ratio as shown in Figure 11(a).

The maximum gain of 14 dBi is achieved for the circularly polarized slotted waveguide array antenna with a radiation efficiency of 95.9%. The pure circular polarization between 276 GHz and 310 GHz is observed from the difference between left-hand circular polarization (LHCP) and right-hand circular polarization (RHCP) as illustrated in Figure 11(b). For the circularly polarized band of frequencies, the minimum magnitude deviation of 10 dBi between LHCP and RHCP is noted. The co-polar and cross-polar radiation patterns at $\varphi = 90°$ and $\varphi = 0°$ are shown in Figure 12(a) and Figure 12(b), respectively.
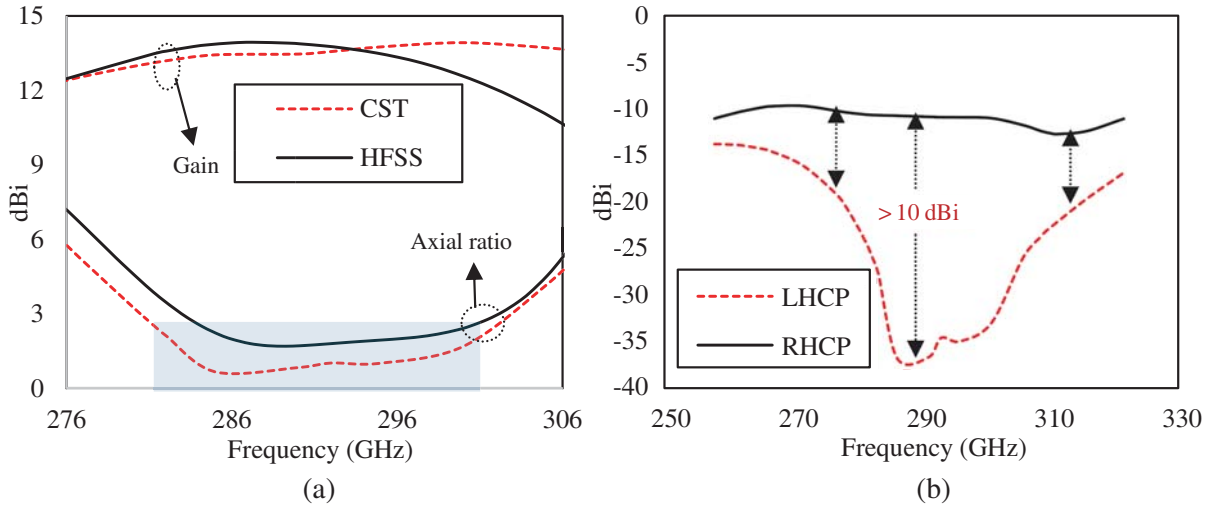
Figure 11. (a) Axial ratio and gain of circularly polarized SLWA are verified in CST and HFSS. (b) The comparison between LHCP and RHCP for the verification of circular polarization.
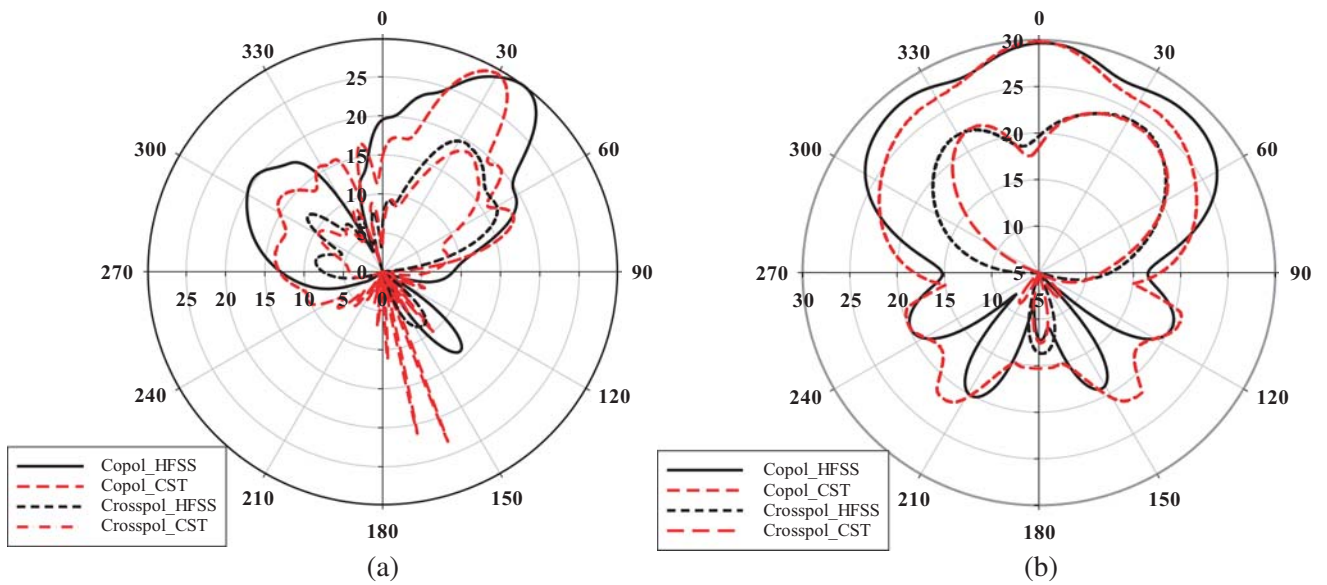

Figure 12. E-Plane pattern for $f = 285\,\text{GHz}$ at (a) $\varphi = 90°$, (b) $\varphi = 0°$ in CST and HFSS.

The circularly polarized polar pattern also shows the broadside radiation towards z-direction with $30°$ shift. The maximum 3 dB beamwidth of $16.177°$ with minimum sidelobe level of $2.5448\,\text{dBi}$ is acquired. The electric field distribution patterns occupied in the cross slots are depicted in Figures 13(a)–(d) for the in-band (28 GHz and 300 GHz) and out-band (260 GHz and 310 GHz) circularly polarized frequencies. Also clockwise rotations of field lines (left hand circular polarization) through the cross section of CRS at 290 GHz (CP frequency) at different phases are represented in Figures 14(a)–(d). The vector fields crossing through the CRS are focussed for both ranges of frequencies at TE_{10} mode. It is observed that the vector field lines deviate from the centre crossing point of the CRS for the out-band CP frequencies. The CP is realized for all the frequencies where electric field lines intersect at the exact centre of CRS. This is because the cross-slot coupling of CRS is accomplished for the circularly polarized radiation throughout the in-band frequencies. The coupling modes of the vertical electric field for the slotted waveguide section are discussed in [16].
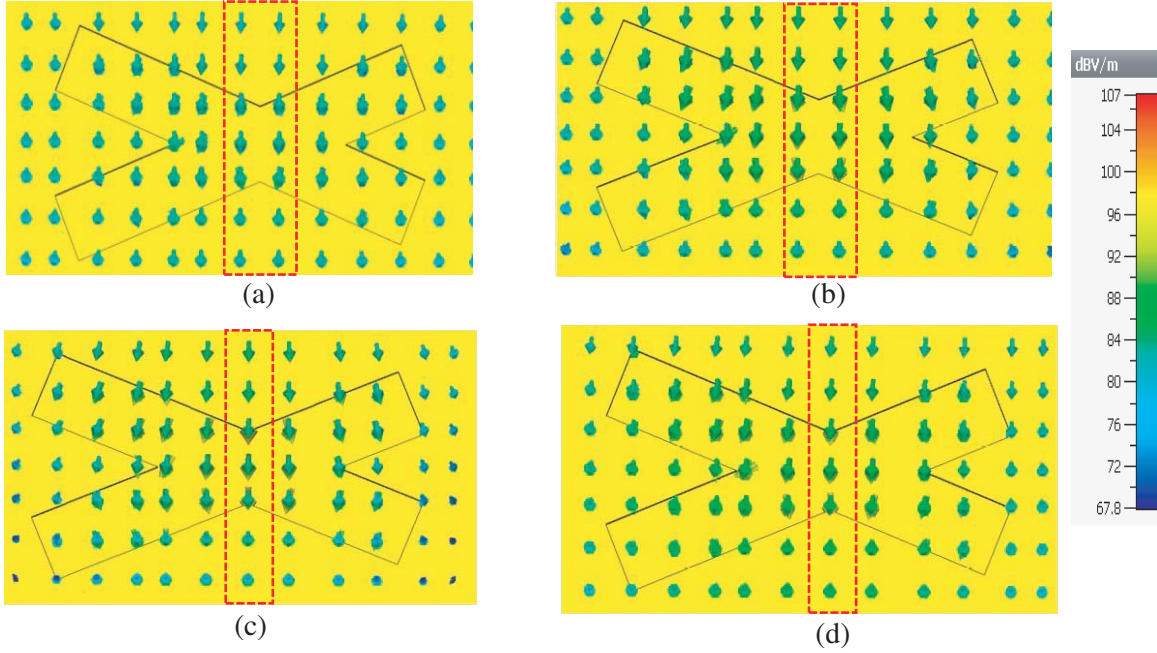
Figure 13. The electric field distribution crossing the CRS. (a) $f = 260\,\text{GHz}$, (b) $f = 310\,\text{GHz}$, (c) $f = 280\,\text{GHz}$, (d) $f = 300\,\text{GHz}$.
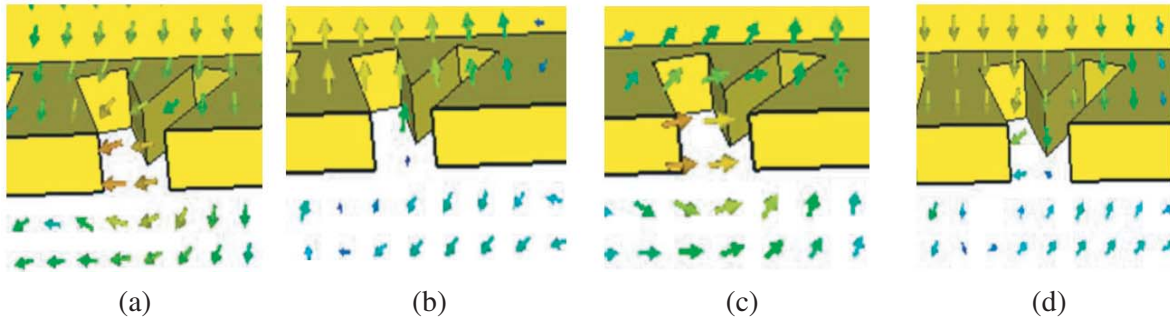

Figure 14. The electric field distribution through the cross sectional view of CRS at $290\,\text{GHz}$. (a) at phase $= 0°$, (b) at phase $= 90°$. (c) at phase $= 180°$, (d) at phase $= 270°$.

4.1. Beam Scanning Slots

4.1.1. Rectangular Stepdown Slots (RSDS)

The linearly polarized slots are modified into rectangular stepdown slots (RSDS) and obtain beam steering for circularly polarized applications. The array is arranged by stepping down the length of each slot in the SLWA inside the metal cabin as illustrated in Figure 15(a). The height of the metal cabin is reduced to 0.5 mm to maintain circular polarization for the beam scanning slots. The broadside array of slots steers the beam at different angles for each resonant frequency of the slotted array.

The designed dimensions for the beam scanning slots are given in Table 3. The maximum gain of 17.1 dBi is realized for the impedance bandwidth of 56.506 GHz (from 253.25 GHz to 309.76 GHz) as observed from Figure 15(b). The control on the boresight directed beam is achieved using the change in frequency. Thereby the beam is shifted by frequency tuning between the upper and lower impedance bandwidth ranges. Beam scans for the angles starting from 17.554°, 22.017°, 27.509°, 30.599°, 34.031°, 36.778°, 39.18°, 42.613°, and 44.33° for frequencies $f_1 = 253\,\text{GHz}$, $f_2 = 260\,\text{GHz}$, $f_3 = 267\,\text{GHz}$, $f_4 = 274\,\text{GHz}$, $f_5 = 281\,\text{GHz}$, $f_6 = 288\,\text{GHz}$, $f_7 = 295\,\text{GHz}$, $f_8 = 302\,\text{GHz}$, and $f_9 = 309\,\text{GHz}$
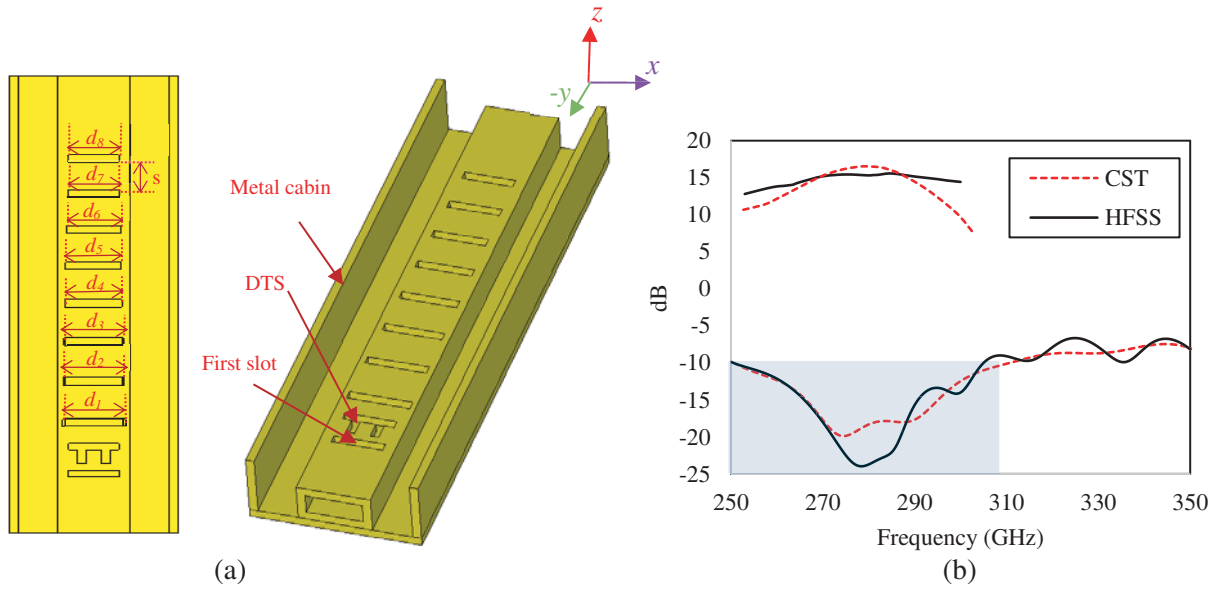
Figure 15. (a) Top view of beam scanning SLWA inside the metal cabin. (b) Reflection coefficient with gain and directivity.
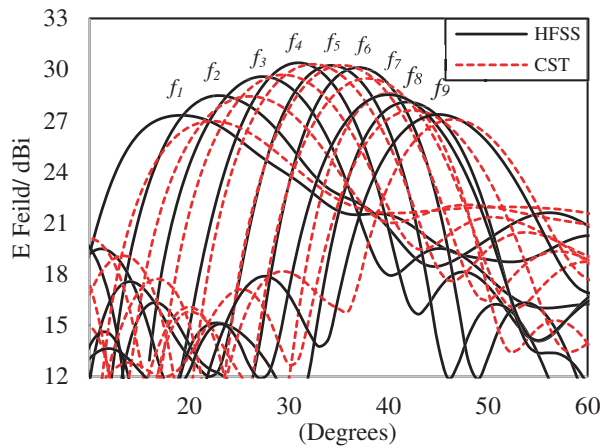

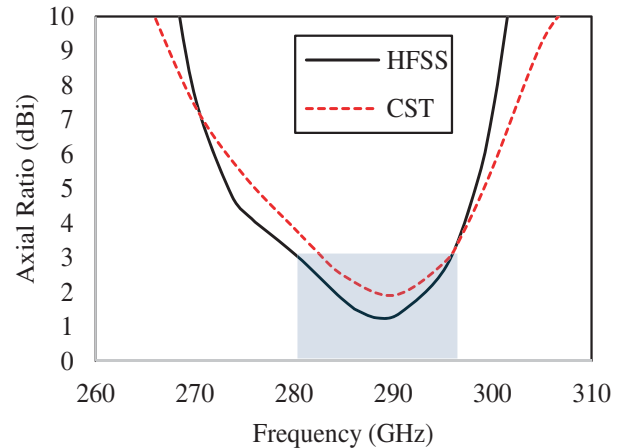**Figure 16.** Beam scanning of SLWA in CST and HFSS.

Figure 17. Axial ratio verification for the beam scanning array of SLWA within the bandwidth.

Table 3. Design of beam scanning slots.

Dimensions	d_1	d_2	d_3	d_4	d_5	d_6	d_7	d_8	s
Values (mm)	0.76	0.74	0.72	0.70	0.68	0.66	0.64	0.62	0.41

respectively given in Figure 16. Although the range of scan angle is limited to $26.784°$, the entire range of angles for frequencies from 250 GHz to 330 GHz can be shifted to the particularly designed bandwidth according to the delicate beam focussing applications. The phase shifting circuits after RSDS SLWA steer the entire narrow beam scan range into the desired direction. The axial ratio is shown in Figure 17 which provides circular polarization from 283 GHz to 295.42 GHz (3 dB AR bandwidth of 12.417 GHz) for the RSDS SLWA. The total radiation efficiency of 96.21% is achieved with the proposed design.

4.1.2. Cross Stepdown Slots (CSDS)

The cross-shaped slot made on the broadwall of the waveguide is a powerful method to achieve circular polarization. The single cross-slot section works on resonant frequency mode and the radiation towards the broadside direction. The array of cross slots on WR3 waveguide utilizes the possibilities of CP as depicted in the CRS part. In order to achieve beam scanning using frequency tuning, the array of cross slots is designed with $-17°$ angular shift, and length of each slot element is decreased homogenously at a distance of 'm' $= 0.3793$ mm as shown in Figure 18. The proposed CSDS has the geometric tolerance of the array element spacing $m < \lambda/2$ with circular polarization, where λ is the free space wavelength.

   The circularly polarized radiation pattern is observed for each beam which is scanned at different frequencies. There is a significant effect of mutual coupling between the adjacent slots. The directive property of DTS provides effective high gain radiation towards boresight direction. Coupling between the slots depends on the active length of the cross elements and the guided wavelength. Maximum bandwidth of 61.236 GHz from 250.53 GHz up to 311.76 GHz is observed in Figure 19 with a maximum gain of 16.1 dBi. Figure 20 illustrates the 3 dB AR bandwidth of 9.688 GHz which is achieved from
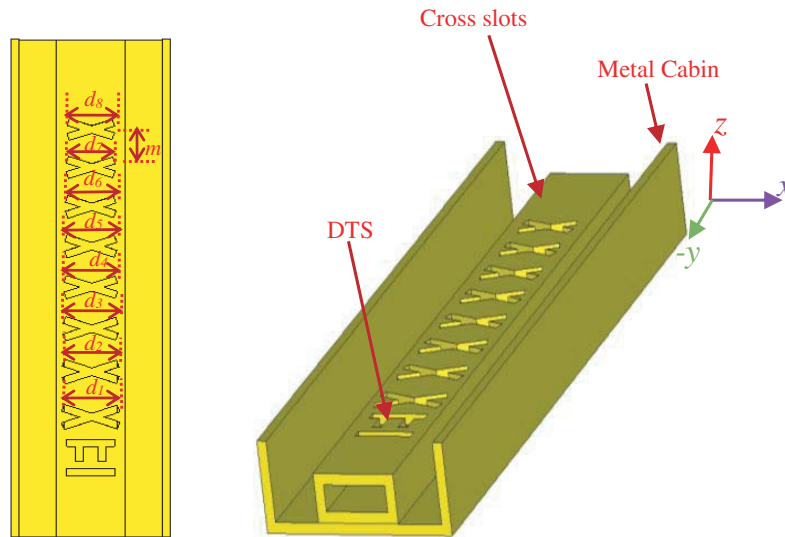

Figure 18. The top view and perspective view of proposed beam-scanning cross slotted SLWA.
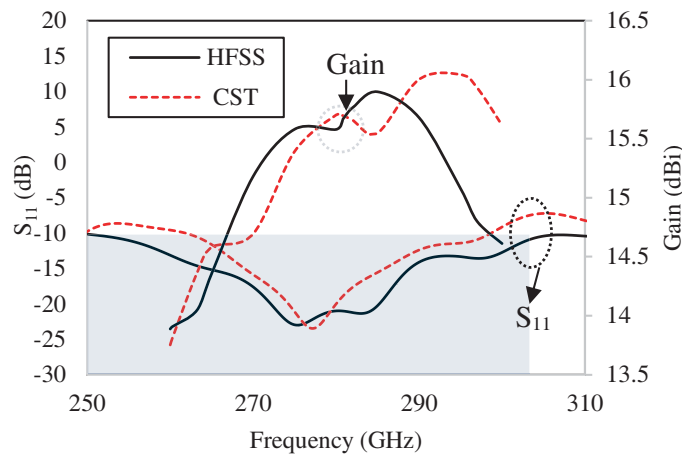

Figure 19. The verification of return loss characteristics of CSDS SLWA along with maximum gain over the bandwidth.
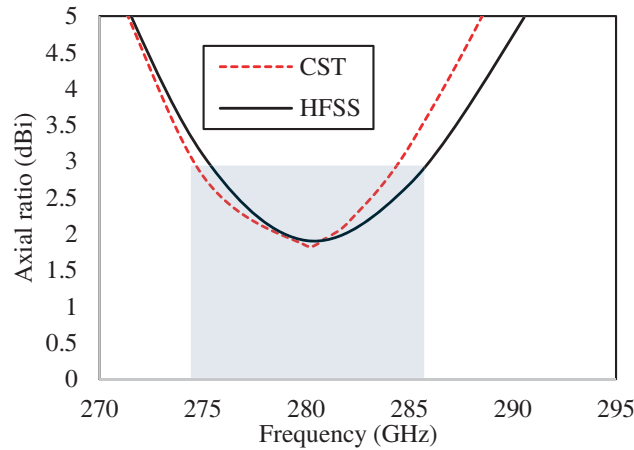
Figure 20. Axial ratio characteristics of CSDS SLWA.

274.67 GHz up to 284.36 GHz with a maximum radiation efficiency of 94.99%. Similar to RSDS, the CSDS also carries a beam towards different angles for the variation in the frequency range according to the dimensions of each slot. The single slotted section itself possesses 35° shift in the main lobe of the radiation pattern. The remaining elements are designed by stepping down the slot length which are responsible for the angular deviation of the radiation beam. The main lobe of the radiation pattern as illustrated in Figure 21 occupies angles 22.156°, 26.173°, 29.46°, 32.3892°, 35.304°, 38.225°, 40.050°, 42.608°, and 45.164° corresponding to the frequencies $f'_1 = 250$ GHz, $f'_2 = 257$ GHz, $f'_3 = 264$ GHz, $f'_4 = 271$ GHz, $f'_5 = 278$ GHz, $f'_6 = 286$ GHz, $f'_7 = 292$ GHz, $f'_8 = 300$ GHz, and $f'_9 = 311$ GHz, respectively. For the metallic waveguide, the metal loss of 2.72% of the accepted power at port-1 is noticed on simulation which is found acceptable for THz frequency range. The results from CST and HFSS are in good agreement in all the frequency scan and reflection characteristics.
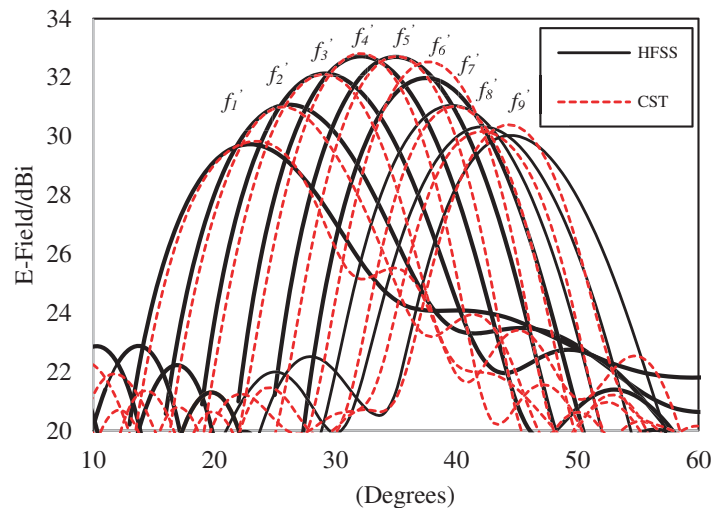
Figure 21. The verification of beam-scanning of CSDS SLWA for the frequencies f'_1 to f'_9.

The circularly polarized antenna parameters such as AR bandwidth, impedance bandwidth, and gain are compared with related high-frequency works of literature and the proposed designs as given in Table 4. The highly efficient circularly polarized SLWA is achieved using CP slots, RSDS, and CSDS with high gain and wide bandwidth. It is observed that 22% fractional bandwidth and high gain are achieved with the proposed design at sub-terahertz frequencies.

Table 4. The comparison between the proposed design and results with other CP literature.

Ref	Structure (frequency)/year	−10 dB Impedance bandwidth range/band (GHz)	3 dB AR Bandwidth range/Band (GHz)	Gain (dBi)	Radiation efficiency (%)
[28]	SIW (60 GHz)/2019	55.5 to 74/18.5	57 to 73/16	10.4	85
[29]	Microstrip antenna (THz)/2019	190 to 240/50	380 to 490/110	6.8	Not mentioned
		270 to 610/340	575 to 590/15		
[30]	Antenna package (60 GHz)/2014	55 to 67/12	54.8 to 68.6/13.8	6	Not mentioned
[31]	LTCC Technology (60 GHz)/2013	57 to 66/9	56 to 64.3/8.3	17.1	Not mentioned
[32]	SIW (Sub-THz)/2014	251.5 to 283.6/32.1	265.6 to 274.5/8.9	−0.5	21.4
This work	1. CRS (Sub-THz)	257 to 321/64	280.89 to 304.21/23.32	14.4	95.9
	2. RSDS (Sub-THz)	253.25 to 309.76/56.51	283 to 295.42/12.42	14	96.21
	3. CSDS (Sub-THz)	250.53 to 311.76/61.23	274.67 to 284.36/9.69	17.1	94.99

5. CONCLUSION

A slotted waveguide array antenna with DTS is designed under sub-THz frequencies for future communications applications. The slots are configured to obtain linear as well as circular polarization, and the slotted waveguide is placed in a metal cabin to increase the maximum gain up to 4 dBi. The reconfiguration of linear polarization into circular polarization is implemented by using modified cross slots and achieves 3 dB AR bandwidth of 23.323 GHz with 95.9% efficiency. Beam scanning is also implemented for the narrow range of scan angle by stepping-down the length of the slot. The designed CP SLWA with RSDS and CSDS provides wide impedance bandwidth and 3 dB AR bandwidth with maximum gain of 17.1 dBi at sub-THz frequencies. The proposed wide circularly polarized beam scanning antennas are highly on demand in the future 5G and 6G communication applications. They are currently approaching upper spectral frequency limits of the radio spectrum towards 300 GHz and even higher THz ranges with novel ways to amplify signals for the enhanced 6G coverage along with the huge amount of data transmission in the upcoming years.

REFERENCES

1. Shkerdin, G., H. Alkorre, H. Guoqiang, and J. Stiens, "Modified TE modes of metal waveguide with integrated graphene structure in the sub-terahertz frequency range," *IET Microwaves, Antennas & Propagation*, Vol. 10, No. 6, 692–699, 2016.
2. Generalov, A. A., J. A. Haimakainen, D. V. Lioubtchenko, and A. V. Räisänen, "Wide band mm- and sub-mm-wave dielectric rod waveguide antenna," *IEEE Transactions on Terahertz Science and Technology*, Vol. 4, No. 5, 568–574, 2014.
3. Tajima, T., H.-J. Song, H. Matsuzaki, and M. Yaita, "LTCC-integrated *H*-plane bends for THz antenna-in-package solution," *IEEE Microwave and Wireless Components Letters*, Vol. 27, No. 5, 440–442, 2017.
4. Tajima, T., H.-J. Song, and M. Yaita, "Compact THz LTCC receiver module for 300 GHz wireless communications," *IEEE Microwave and Wireless Components Letters*, Vol. 26, No. 4, 291–293, 2016.

5. Tajima, T., H.-J. Song, K. Ajito, M. Yaita, N. Kukutsu, "300-GHz step-profiled corrugated horn antennas integrated in LTCC," *IEEE Transactions on Antennas and Propagation*, Vol. 62, No. 11, 5437–5444, 2014.

6. Patidar, D., P. K. Singhal, H. K. Gupta, and G. Sharma, "Microstrip planner five-element Yagi-Uda antenna for ISM band application," *International Journal of Engineering and Technology*, Vol. 1, No. 4, 395–400, 2012.

7. Cai, R.-N., M.-C. Yang, S. Lin, X.-Q. Zhang, X.-Y. Zhang, and X.-F. Liu, "Design and analysis of printed yagi-uda antenna and two-element array for WLAN applications," *International Journal of Antennas and Propagation*, 1–8, 2012.

8. Rodriguez-Ulibarri, P. and T. Bertuch, "Microstrip-fed complementary Yagi-Uda Antenna," *IET Microwaves, Antennas & Propagation*, Vol. 10, No. 9, 926–931, 2016.

9. King, R. W. P. and S. S. Sandler, "The theory of broadside arrays," *IEEE Transactions on Antennas and Propagation*, 269–275, May 1964.

10. Guglielmi, M. and D. R. Jackson, "Broadside radiation from periodic leaky-wave antennas," *IEEE Transactions On Antennas And Propagation*, Vol. 41, No. I, 31–37, 1993.

11. Comite, D., S. K. Podilchak, P. Baccarelli, P. Burghignoli, A. Galli, A. P. Freundorfer, and Y. M. M. Antar, "Analysis and design of a compact leaky-wave antenna for wide-band broadside radiation," Nature Scientific Reports, Vol. 8, No. 17741, 4–14, 2018.

12. Bayat-Makou, N., K. Wu, and A. A. Kishk, "Single-layer substrate-integrated broadside leaky long-slot array antennas with embedded reflectors for 5G systems," *IEEE Transactions on Antennas And Propagation*, Vol. 67, No. 12, 7331–7339, Dec. 2019.

13. Hesariand, S. S. and J. Bornemann, "Wideband circularly polarized substrate integrated waveguide end-fire antenna system with high gain," *IEEE Antennas and Wireless Propagation Letters*, Vol. 16, 2262–2265, 2017.

14. Wang, A., L. Yang, Y. Zhang, Xi Li, X. Yi, and G. Wei1, "A novel planar dual circularly polarized endfire antenna," *IEEE Access*, Vol. 7, 64297–64302, 2019.

15. Abdelrahim, W. and Q. Feng, "Compact broad band dual-band circularly polarised antenna for universal UHF RFID handheld reader and GPS applications," *IET Microwaves, Antennas & Propagation*, Vol. 13, No. 10, 1664–1670, 2019.

16. Lu, W. J., K. Wang, S.-S. Gu, L. Zhu, and H. Bo. Zhu, "Directivity enhancement of planar endfire circularly polarized antenna using V-shaped 1.5-wavelength dipoles," *IEEE Antennas and Wireless Propagation Letters*, Vol. 18, No. 7, 1420–1423, 2019.

17. Liu, J., H. Lu, Z. Li, Z. Liu, Z. Dong, C. Deng, X. Lv, and Y. Liu, "Wideband circularly polarized waveguide-fed antipodal exponential tapered slot antenna," *IEEE Antennas and Wireless Propagation Letters*, Vol. 18, No. 9, 1912–1916, 2019.

18. Wang, M., L. Hu, J. Chen, S. Qi, and W. Wu, "Wideband circularly polarized square slot array fed by slotted waveguide for satellite communication," *Progress In Electromagnetics Research Letters*, Vol. 61, 111–118, 2016.

19. Li, G., H. Zhai, T. Li, L. Li, and C. Liang, "CPW-fed S-shaped slot antenna for broad band circular polarization," *IEEE Antennas and Wireless Propagation Letters*, Vol. 12, 619–622, 2013.

20. Salari, M. and M. Movahhedi, "A new configuration for circularly polarized waveguide slot antenna," *Proceedings of The Asia-Pacific Microwave Conference*, 606–609, 2011.

21. Stilwell, R. K., R. E. Wallis, and M. L. Edwards, "A circularly polarized, electrically scanned slotted waveguide array suitable for high temperature environments," *IEEE Antennas and Propagation Society International Symposium, Digest*, 1030–1033, Held in Conjunction With: Usnc/Cnc/Ursi North American Radio Sci. Meeting, 2003.

22. Zhao, Y., K. Wei, Z. Zhang, and Z. Feng, "A waveguide antenna with bidirectional circular polarizations of the same sense," *IEEE Antennas and Wireless Propagation Letters*, Vol. 12, 559–562, 2013.

23. Wu, X., F. Yang, F. Xu, and J. Zhou, "Circularly polarized waveguide antenna with dual pairs of radiation slots at Ka-band," *IEEE Antennas and Wireless Propagation Letters*, Vol. 16, 2947–2950, 2017.

24. Xu, J., M. Wang, H. Huang, and W. Wu, "Circularly polarized patch array fed by slotted waveguide," *IEEE Antennas and Wireless Propagation Letters*, Vol. 14, 8–11, 2015.

25. Xia, F. Y., Y. J. Cheng, Y. F. Wu, and Y. Fan, "V-band wideband circularly polarized endfire multibeam antenna with wide beam coverage," *IEEE Antennas and Wireless Propagation Letters*, Vol. 18, No. 8, 1616–1620, 2019.

26. Shang, Y., H. Yu, H. Fu, and W. M. Lim, "A 239–281 GHz CMOS receiver with on-chip circular-polarized substrate integrated waveguide antenna for sub-terahertz imaging," *IEEE Transactions on Terahertz Science and Technology*, Vol. 4, No. 6, 686–695, 2014.

27. Ansari, M., H. Zhu, N. Shariati, and Y. J. Guo, "Compact planar beamforming array with endfire radiating elements for 5G applications," *IEEE Transactions on Antennas and Propagation*, Vol. 67, No. 11, 6859–6869, 2019.

28. Elhefnawy, M. and A. A. Al-Hadi, "A novel design of slotted waveguide phased array antenna," *Advanced Electromagnetics*, Vol. 8, No. 3, 16–22, 2019.

29. Nisamol, T. A., K. K. Ansha, and P. Abdulla, "Design of sub-THz beam scanning antenna using Luneburg lens for 5G communications or beyond," *Progress In Electromagnetics Research C*, Vol. 99, 179–191, 2020.

30. Ghasemi, A. and J.-J. Laurin, "A continuous beam steering slotted waveguide antenna using rotating dielectric slabs," *IEEE Transactions on Antennas and Propagation*, Vol. 67, No. 10, 6362–6370, 2019.

31. Lu, L., et al., "Design of low-sidelobe circularly polarized loop linear array fed by the slotted SIW," *IEEE Antennas and Wireless Propagation Letters*, Vol. 16, 537–540, 2016.

32. Shang, X., M. Ke, Y. Wang, and M. J. Lancaster, "WR-3 band waveguides and filters fabricated using SU8 photoresist micromachining technology," *IEEE Transactions on Terahertz Science and Technology*, Vol. 2, No. 6, 629–637, 2012.

33. Russo, I., L. Boccia, G. Amendola, and H. Schumacher, "Compact hybrid coaxial architecture for 3 GHz–10 GHz UWB quasi-optical power combiners," *Progress In Electromagnetics Research*, Vol. 122, 77–92, 2012.